Cavendish-HEP-07/09

Edinburgh 2007/21

Loop induced interference effects in Higgs Boson plus two jet production at the LHC

J. R. Andersen[a], T. Binoth[b], G. Heinrich[b], J. M. Smillie[a]

[a]Cavendish Lab, JJ Thomson Avenue, Cambridge, CB3 0HE, UK
[b]School of Physics, The University of Edinburgh, Edinburgh EH9 3JZ, UK

February 22, 2008

Abstract

We calculate the order $\mathcal{O}(\alpha^2\alpha_s^3)$ interference effect between the gluon fusion and weak boson fusion processes allowed at the one-loop level in Higgs boson plus 2 jet production at the LHC. The corresponding one-loop amplitudes, which have not been considered in the literature so far, are evaluated analytically using dimensional regularisation and the necessary master integrals with massive propagators are reported. It is discussed in detail how various mechanisms conspire to make this contribution numerically negligible for experimental studies at the LHC.

1 Introduction

One of the main tasks for the experimental and theoretical programme in connection with the CERN LHC is to investigate the mechanism of electro-weak symmetry breaking. Central to this study would be the measurement of the couplings of any observed Higgs scalar to the electro-weak bosons. This can be performed either by studying the decays $H \to ZZ, WW$ [1, 2] with contributions from all production channels, or the production process $pp \to Hjj$ [3–5] through weak boson fusion (WBF) [6], as shown in Fig. 1(a), with contributions from all identifiable decay channels. The Higgs plus two jet signature also receives contributions from Higgs boson production through gluon-fusion mediated through a top-loop, as illustrated in Fig. 1 (b). However, the Higgs plus dijet-sample can be biased towards WBF by suppressing the gluon-fusion channel through a combination of cuts, requiring both well-separated jets (effectively suppressing the largest component of gluon-initiated processes) and suppressing events with further central jets (produced predominantly in the gluon-fusion channel, since here the two tagging jets are colour-connected).

For the gluon fusion process, the first radiative corrections have been calculated within QCD [7, 8] using the heavy top mass effective Lagrangian [9–11]. For the WBF, both the radiative corrections within QCD [11–14] and the electro-weak sector [15] have been calculated.

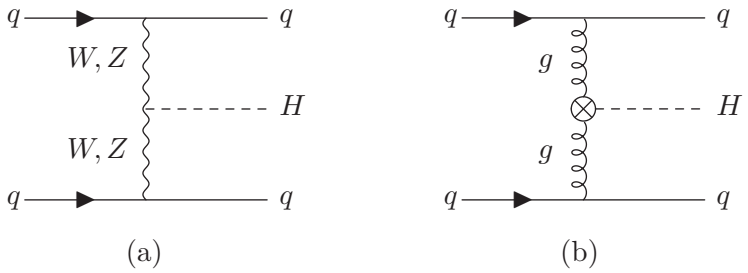

Figure 1: (a) The WBF process for Higgs production in the Standard Model and (b) the equivalent gluon-fusion diagram mediated through a top-loop.

The radiative corrections to the WBF channel are small, $3\% - 6\%$, and there is even partial numerical cancellation between the QCD and electro-weak contributions. It would therefore seem that the Higgs coupling to electro-weak bosons can be very cleanly studied with a Hjj-sample.

Until recently, the irreducible contamination in the extraction of the ZZH-coupling from interference between the gluon fusion and WBF processes was ignored in the literature. At tree level, such interference is only allowed in amplitudes where the two quarks have the same flavours, but their contribution is kinematically suppressed by the requirement of a $t \leftrightarrow u$-channel crossing, as discussed in Ref. [16]. These interference terms were later also included in the calculation reported in Ref. [15], where the full electroweak corrections have been calculated, and which also took into account other crossing-suppressed one-loop amplitudes.

In the present paper we will report on the calculation of the processes allowed at the one-loop level which do not suffer from the suppression stemming from the requirement of a $t \leftrightarrow u$-crossing. As will be explained below, one finds at order $\mathcal{O}(\alpha^2\alpha_s^3)$ an interference term between the gluon- and Z-induced amplitude which is not allowed at $\mathcal{O}(\alpha^2\alpha_s^2)$ by colour conservation. The W-induced amplitudes are crossing-suppressed and therefore not taken into account. The diagrams where the vector boson is in the s-channel can be safely neglected because they are strongly suppressed by the WBF cuts.

Given that electroweak corrections to the WBF process, which are formally an order $\mathcal{O}(\alpha)$ correction to an $\mathcal{O}(\alpha^4)$ process, have been shown to be relevant for this important process [15], simple power counting alone suggests that the size of the irreducible contamination due to the discussed interference effect should be checked. We will elaborate below that arguments in the literature which are based on simplified assumptions do not capture all effects found by doing the full one-loop calculation.

In the following section we will briefly sketch the calculation before discussing our results in section 3, which are summarized in the conclusions. The appendix contains an extensive list of the master integrals needed for this calculation. Most of these integrals have not been reported in the literature so far.

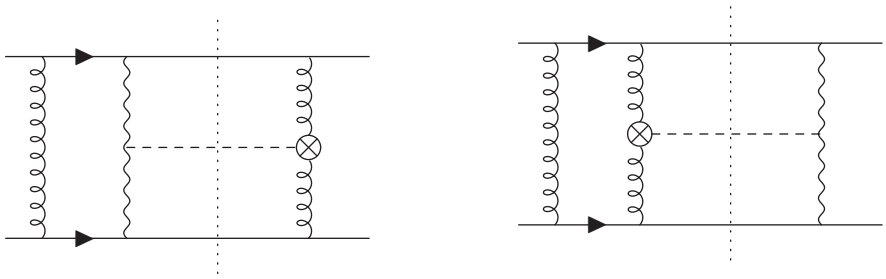

(a) (b)

Figure 2: Example of contributing one-loop interference terms: (a) $\mathcal{M}_{gZ}\mathcal{M}_g^*$ and (b) $\mathcal{M}_{gg}\mathcal{M}_Z^*$. There are four contributing topologies for each gluon-fusion and Z-fusion process.

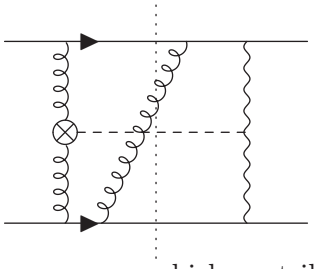

Figure 3: One of the real emission processes which contributes at the matrix element squared level.

2 The Calculation

We set out to calculate the helicity amplitudes necessary to form the loop interference terms and the real emission contributions. Sample diagrams are shown in Figs. 2 and 3. As discussed in Ref. [16] this is the lowest order contribution to the interference between ZZH and ggH-processes for non-identical quark flavours and helicity configurations, and for identical quark and helicity configurations the loop amplitudes are the first order which does not require a kinematically disfavoured crossing.

The amplitudes have four non-zero helicity components, which we label by $++++$, $----$, $-++-$ and $+--+$. Due to parity invariance of the kinematical part of the amplitudes, only two of them are independent. By using the spinor helicity formalism we have defined projection operators on each of these amplitudes. In practice, we calculate the amplitudes with all momenta incoming (and therefore summing to zero); to map to physical scattering kinematics, crossing relations are applied easily in the end.

The leading order amplitudes, denoted by $\mathcal{M}_Z$ and $\mathcal{M}_g$ (see Fig. 2), are proportional to a colour singlet and a colour octet term. The colour singlet is formally of order $\mathcal{O}(\alpha^2)$ whereas the octet is of order $\mathcal{O}(\alpha_s^2)$. The virtual corrections, which we call $\mathcal{M}_{gZ}$ and $\mathcal{M}_{gg}$ respectively,

are mixtures of octet and singlet terms. For the intereference term we need to consider only the octet part of $\mathcal{M}_{gZ}$ and the singlet part of $\mathcal{M}_{gg}$. One finds that only four one-loop five-point topologies for each amplitude survive this colour projection. As was already pointed out in Ref. [16], the colour singlet cannot interfere with the colour octet tree amplitude for different quark flavours. However, a new colour channel opens up at order $\mathcal{O}(\alpha^2\alpha_s^3)$ which is neither flavour nor kinematically suppressed.

The loop amplitudes require the evaluation of one-loop five-point tensor integrals with partly massive propagators and external legs. We apply the reduction algorithm outlined in Ref. [17,18] to express each Feynman diagram as a linear combination of 1-, 2-, and 3-point functions in $D = 4-2\epsilon$ dimensions and 4-point functions in D=6. The same algorithm has been successfully applied to a number of one-loop computations and further details can be found elsewhere [19–22]. The coefficient of each integral, which is a rational polynomial in terms of Mandelstam variables $s_{ij} = (p_i + p_j)^2$ and masses, was evaluated symbolically using FORM [23] and simplified using MATHEMATICA [24]. Both steps were fully automated. The algebraic expressions were checked by independent implementations, both amongst the authors and with another group [25].

After the algebraic reduction, all helicity amplitudes for both cases, gluon and weak boson fusion, were obtained as linear combinations of a certain number of scalar integrals. We choose this basis of so-called master integrals (MIs) in accordance with Ref. [26], i.e. our MI's are D-dimensional two-point and three-point functions (I_2^D, I_3^D), and (D+2)-dimensional four-point functions (I_4^{D+2}). Schematically

$$\mathcal{M} = \sum_{j,\alpha} k_{j\alpha} I_j(\{s_\alpha, m_\alpha\}) \;, \quad I_j \in \{I_2^D, I_3^D, I_4^{D+2}\} \tag{1}$$

where the summation over α indicates the summation over different argument lists $\{s_\alpha, m_\alpha\}$ of the relevant MI. The conventions for the arguments and the analytic forms of these are given in the appendix. No one-point functions appear in the reduction, and also two-point functions are absent in the amplitudes of $\mathcal{M}_{gZ}$. Furthermore, coefficients of some of the integrals which arise in several topologies sum to zero: if the tree resulting from a cut of an internal line of a master integral corresponds to helicity forbidden tree level processes one can immediately infer the vanishing of the corresponding coefficient. In our algebraic tensor reduction approach we are able to verify such cancellations and enforce them analytically before the numerical evaluation of the cross section (for a nontrivial example see Ref. [26]).

The coefficients we obtain through this procedure can be too large to be of use in a printed form (their simple polynomial structure means that numerical evaluation is, however, fast). We performed several algebraic checks of relations between coefficients of different topologies and helicity configurations. The coefficients are included as supplementary material to this paper.

As most of the required integrals are not provided in the literature, we have evaluated representations in terms of analytic functions valid in all kinematic regions. We give our result

p_{a_T}, p_{b_T}	> 20 GeV	$\eta_a \cdot \eta_b$	< 0
η_j	< 5	$\lvert\eta_a - \eta_b\rvert$	> 4.2
s_{ab}	$> (600\ \text{GeV})^2$		

Table 1: The cuts used in the following analysis which bias the Higgs Boson plus dijet sample towards WBF. The suffices a, b label the tagged jets.

for these integrals in the appendix, as they might be of use for other calculations[1].

The IR structure of the interference term is very simple. It is easily extracted from the result by focusing on the IR divergent triangles. All MIs with single poles drop out. Only triangles with double poles survive. This results in an expression

$$\sim \alpha_s C_F[(-s_{13})^{-\epsilon} + (-s_{24})^{-\epsilon} - (-s_{12})^{-\epsilon} - (-s_{34})^{-\epsilon}]/\epsilon^2$$

in which all double poles cancel and only sub-leading soft divergences survive.

The virtual corrections to the interference term have to be combined with the real emission part shown in Fig. 3. In accordance with the virtual corrections, the collinear IR divergences from the three-parton final states integrate to zero, leaving only a soft divergence proportional to $1/\varepsilon$ in dimensional regularisation. Due to the simple structure of the divergences, we have used the phase space slicing method [28,29] to isolate the IR divergences from the real radiation part. We have checked that the remaining single poles cancel exactly when combining the real emission with the virtual part. The phase space integration and the numerical evaluation of integrals and coefficients is coded in a C++ program allowing for a flexible implementation of cuts and observables.

3 Results

This study aims at investigating a possible pollution of the clean extraction of the ZZH vertex structure by the interference terms. Therefore we will apply the cuts summarised in Table 1, which are generally used for the selection of WBF events [30] over the gluon fusion "background". Our input parameters for the numerical studies are taken from either the parton density function-fit [31] in the case of $\alpha_S(M_Z^2)$ and the Review of Particle Physics [32] for the others.

$$\begin{aligned} &\alpha_s(M_Z^2) = 0.1205\,, \qquad g^2 = \frac{G_F}{\sqrt{2}}\frac{1}{8M_W^2}\,, \qquad G_F = 1.16637 \times 10^{-5}\ \text{GeV}^{-2} \\ &M_Z = 91.1876\ \text{GeV}\,, \quad M_W = 80.425\ \text{GeV}\,, \quad \sin^2\theta_W = 0.2312\,. \end{aligned} \tag{2}$$

[1] Of course all finite integrals can in principle be evaluated by using the LoopTools package [27]. The $D = 6$ boxes can be written as linear combinations of 3- and 4-point functions in D=4. If IR divergences are present, a small regulator mass must be used, but its dependence can be made arbitrarily small as the D=6 box integral is IR finite.

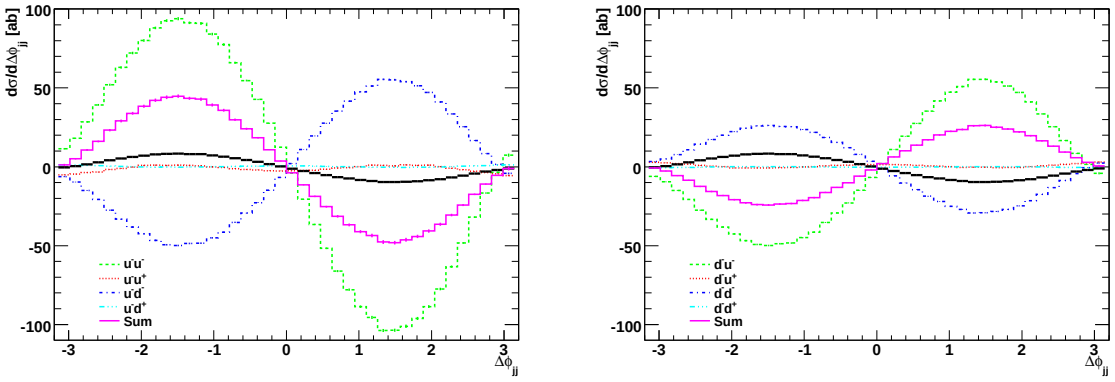

Figure 4: The $\Delta\phi_{jj}$-distribution for different helicity-configurations of the valence quarks only. The purple histogram labelled "Sum" indicates the sum over the four contributions shown. The sum over *all* valence quark flavour and helicity assignments is shown in the black histogram.

We have checked that variations of the numerical values chosen for the WBF cuts have no impact on the conclusions, nor does the exact value of the Higgs boson mass, which we set to 115 GeV unless otherwise stated. The same is true for the choice of parton sets; we choose to use the NLO set from Ref. [31], and use 2-loop running for α_s, in accordance with the chosen pdfs.

We observe that in all the flavour and helicity channels, the finite contribution from the 3-parton final state is numerically negligible. In fact, in the case at hand, the only rôle of this real emission is to cancel the divergences which arise from the one-loop diagrams.

As an interference effect proportional to $2\mathrm{Re}(\mathcal{M}_{gg}\mathcal{M}_Z^* + \mathcal{M}_{gZ}\mathcal{M}_g^*)$, the result is not necessarily positive definite. In fact, the sign of the interference contribution depends on the azimuthal angle between the two tagging jets, $\Delta\phi_{jj}$. Because of the event topology with two well separated jets, it becomes possible to define an orientation of the azimuthal angle which allows observability in the whole range of $[-\pi, \pi)$, as pioneered in Ref. [6, 33]. $\Delta\phi_{jj}$ is then defined through

$$\begin{aligned} |p_{+_T}||p_{-_T}|\cos\Delta\phi_{jj} &= p_{+_T}\cdot p_{-_T}, \\ 2|p_{+_T}||p_{-_T}|\sin\Delta\phi_{jj} &= \varepsilon_{\mu\nu\rho\sigma} b_+^\mu p_+^\nu b_-^\rho p_-^\sigma, \end{aligned} \tag{3}$$

where b_+ (b_-) are unit vectors in positive (negative) beam direction, and likewise for the jet momenta $p_\pm$. The cuts ensure that the two tagging jets lie in opposite hemispheres.

Figure 4 displays the contribution to the distribution in $\Delta\phi_{jj}$ from the interference terms for various helicity and flavour configurations of the valence quarks only, for a Higgs boson mass of 115 GeV. Figure 5 displays the contribution to the distribution in $\Delta\phi_{jj}$ including sea quarks.

Due to the oscillatory behaviour, the total integrated cross section does not at all tell the full story about the size of the impact on the $\Delta\phi_{jj}$-distribution; for example, the integral of

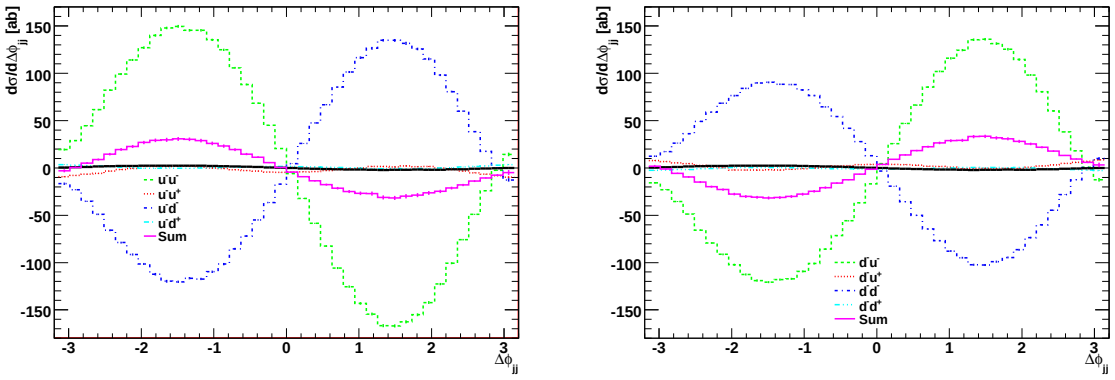

Figure 5: The $\Delta\phi_{jj}$-distribution for various flavour and helicity-configurations. The purple histogram labelled "Sum" indicates the sum over the four contributions shown. The sum over *all* flavour and helicity assignments including all sea flavours is shown in the black histogram.

the contribution from the sea and valence up-quarks with negative helicity, denoted by u^-u^-, is +5 ab, while the distribution peaks at more than 150 ab/rad. If only valence quarks are considered, the integral is −30 ab, while the distribution peaks at ~ 90 ab/rad.

There is an accidental cancellation of sea and valence quark contributions which leads to the fact that the sum over all flavour and helicity assignments peaks at around 2 ab/rad only, with an integrated effect of 1.19 ± 0.07 ab, where the error is due to the numerical integration. Note that the integral of the absolute value of the ϕ_{jj} distribution,

$$\int_{-\pi}^{\pi} d\Delta\phi_{jj} \left| \frac{d\sigma}{d\Delta\phi_{jj}} \right| \ ,$$

is a useful measure of the impact of the interference effect on the extraction of the ZZH-vertex. This integral evaluates to 9.1 ± 0.1 ab, an order of magnitude larger. The total integral over the the absolute value of the fully differential cross section leads to 29.59 ± 0.07 ab.

As can be readily seen, there is a cancellation between the contribution from each flavour and helicity assignment; this is because the sign of quark couplings to the Z-boson becomes relevant, since it is not squared for the interference. The flavour- and helicity sum for each quark line therefore leads to some cancellation, resulting from the weak charges listed in Table 2. This cancellation was discussed in Ref. [34] for the valence content where it was pointed out that if $\sin^2\theta_W = 1/4$ and the u-valence content of the proton was exactly twice the d-valence content for all Björken x, the contributions from uu, ud and dd would sum to zero. However, neither of these approximations is exactly true: $\sin^2\theta_W = 0.2312$ and the parton distribution functions are shown in Fig. 6. The cancellation stemming from the $SU(2) \times U(1)$-flavour and helicity sums

q_λ	$a_{f,\lambda}$	$b_{f,\lambda}$
u_L	1/2	-2/3
u_R	0	-2/3
d_L	-1/2	1/3
d_R	0	1/3

Table 2: $SU(2) \times U(1)$ charges for the $Zq\bar{q}$-couplings, $[a_{f,\lambda} + b_{f,\lambda}\ \sin^2(\theta_W)]$

of the valence quarks can be effectively studied by calculating the ratio

$$\begin{aligned} &\sum_{f,\lambda} c_{f,\lambda}(x,Q^2) / \sum |c_{f,\lambda}(x,Q^2)| \qquad \text{where} \\ &c_{f,\lambda}(x,Q^2) = f(x,Q^2)\ [a_{f,\lambda} + b_{f,\lambda}\ \sin^2(\theta_W)], \end{aligned} \tag{4}$$

where $f(x,Q^2)$ is the relevant parton distribution function. This ratio is plotted in Fig. 7 (left). This figure also shows the ratio of the u-valence to the d-valence pdf, which influences the cancellation. It follows that in QCD the cancellation due to $SU(2) \times U(1)$-flavour and helicity traces amounts to roughly 10^{-1} in the most relevant regions of the pdfs[2]. If one includes the sea quarks in this argument, one sees that the ratio Eq. (4) is modified significantly, see Fig. 7 (right). Its change of sign in the relavant x-region leads to a further reduction of the interference term after integration.

Using the same cuts and value for the mass of the Higgs boson as in the present study, we have checked that the total contribution to the $\Delta\phi_{jj}$-distribution from the leading order WBF process (both Z and $W^{+/-}$ included) is relatively flat at around 240 fb/rad. Therefore, the result of the interference effect reported here is unlikely to be measurable.

The smallness of the overall effect is in fact also a result of the complex phases arising from the full one-loop calculation of the amplitudes. To illustrate this, we calculate the average value of

$$\frac{|\mathrm{Re}\left(\mathcal{M}_{gZ}\mathcal{M}_g^* + \mathcal{M}_{gg}\mathcal{M}_Z^*\right)|}{|\mathcal{M}_{gZ}\mathcal{M}_g^*| + |\mathcal{M}_{gg}\mathcal{M}_Z^*|}. \tag{5}$$

The average over phase space for this quantity is roughly 20%, which illustrates that the relevant products and sums for the interference effect project out only a small component of the full complex loop amplitudes.

We have checked that none of the sources of suppression discussed above depends severely on the mass of the Higgs boson; since the amplitudes themselves depend on this parameter only weakly, the effect of increasing the Higgs boson mass is basically nothing but a reduction

[2]We were not able to reproduce the one order of magnitude larger suppression factor reported in Ref. [34] within the naive Quark Model.

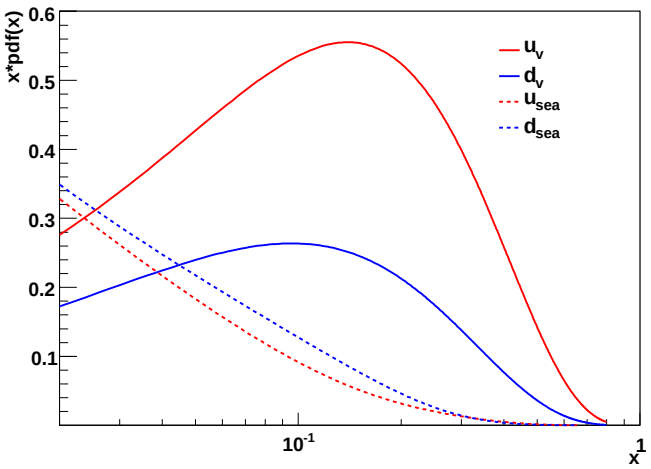

Figure 6: The required parton distribution functions [31] in the relevant region of Björken x for $Q^2 = 400$ GeV^2.

of available phase space. This reduction however is very small, since the partonic centre of mass energy is dominated by the contribution from the jets rather than the Higgs boson. The exact numerical value chosen for the cuts also does not affect the relative importance of the interference effect — the effect on the interference and the WBF signal is similar, so the relative importance of the interference is largely unchanged.

For completeness we list in Table 3 the integral of the absolute $\Delta\phi_{jj}$-distribution for various choices of the renormalisation and factorisation scales.

We chose the factorisation and renormalisation scales as in accordance with the natural scales in the relevant high energy limit (as in Ref. [35]), i.e. the factorisation scales are set equal to the

$\mu_{f,a} = \mu_{r,a}$	$\mu_{f,b} = \mu_{r,b}$	Integral of $\lvert d\sigma/d\Delta\phi_{jj}\rvert$[ab]
p_{a_T}	p_{b_T}	9.1 ± 0.1
$m_H/2$	$m_H/2$	13.9 ± 0.6
m_H	m_H	9.2 ± 0.4
$2m_H$	$2m_H$	6.3 ± 0.3

Table 3: The dependence of the interference effect on the choices for factorisation and renormalisation scales, with a fixed mass of the Higgs boson of 115 GeV. The variation is slightly larger than what would be expected from renormalisation scale variations only, since the variations in factorisation scale impacts the cancellations between $SU(2) \times U(1)$-charges by slightly altering the ratio defined above Eq. (4).

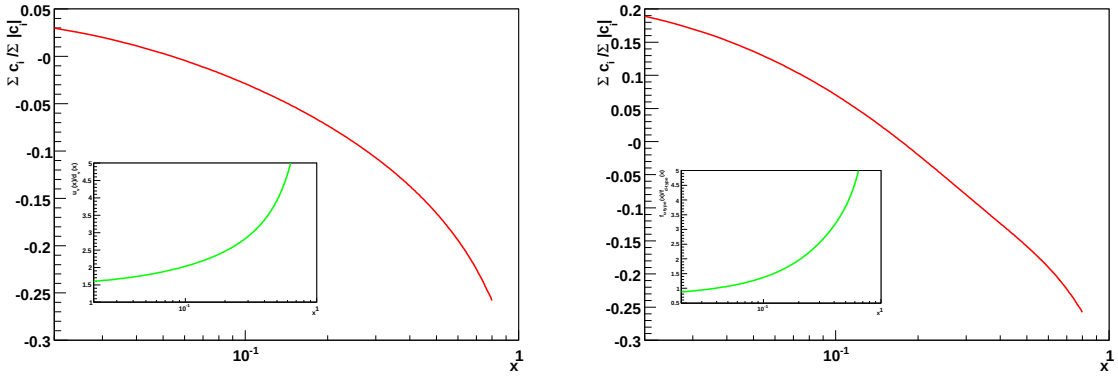

Figure 7: The pdf-weighted sum of the $SU(2) \times U(1)$-charges divided by the sum of the absolute weighted charges for valence quarks only (left) and valence and sea quarks (right). The left figure illustrates how the apparent almost complete cancellation expected from the Quark Model is in fact not as severe once the pdfs are taken into account, as discussed in the text. The insert shows the ratio of the valence u-quark distribution to the valence d-quark distribution for the pdf set MRST 2004 (NLO) [31]. The right plot shows that the inclusion of sea quarks does actually alter the pdf-weighted sum in the relevant x range such that there are additional compensations when integrating over x.

transverse momenta of the relevant jet, and the renormalisation scale for the strong couplings are chosen correspondingly, i.e. one α_s evaluated at each value of the transverse momentum of the jets, and one at the Higgs mass. However, varying these has no impact on the conclusions.

4 Conclusions

We have presented the calculation of the loop-induced $\mathcal{O}(\alpha^2\alpha_s^3)$ interference effect between the gluon fusion and weak boson fusion processes in Higgs boson plus two jet production at the LHC.

In the context of the weak boson fusion cuts we have evaluated all relevant one-loop diagrams algebraically and have obtained an analytic representation of the interference term as a linear combination of scalar one-loop integrals. The analytic result for all the necessary integrals is presented for general kinematics such that it can be used in other computations.

Our expressions have been coded into a flexible computer program to test speculations in the literature about the size of this interference contribution. We do confirm by explicit calculation that this contribution is too small to contaminate the extraction of the ZZH-coupling from WBF processes. Interestingly the effect which survives comes dominantly from the virtual corrections.

We have analysed in detail why this contribution is so small, and instead of a single effect we rather find a conspiracy of several mechanisms which can only be completely assessed having the full NLO calculation at hand.

The mechanisms basically are

- accidental cancellations between the sea quark and valence quark contributions
- compensations between different weak isospin flavours of the valence quark contributions due to their $SU(2) \times U(1)$ couplings in combination with their weights from the (valence) quark content of the proton
- cancellations due to destructive interference of the phases from the different contributions.

The exact impact of these partly accidental effects has until now not been quantified thoroughly and was very hard to assess without an explicit calculation.

As a final comment we would like to point out that anomalous couplings which affect the phases could change the interference pattern substantially. However, the first two cancellation mechanisms still being present, the overall contribution is still expected to be undetectably small.

Acknowledgements

We would like to thank Lance Dixon for enlightening and encouraging discussions and important comments. The authors were all supported by the UK Science and Technology Facilities Council. In addition, the work of TB was supported by the Deutsche Forschungsgemeinschaft (DFG) under contract number BI 1050/2 and the Scottish Universities Physics Alliance (SUPA).

A Analytic Results for Master Integrals

The appendix contains the Master Integrals (MIs) which occur in the reduction of the one-loop pentagon diagrams encountered in the given calculation. The analytic results of the integrals containing only massless propagators have appeared in the literature, see e.g. [17,36–38]. Those with massive propagators have been calculated for this project. All finite integrals can also be calculated by the `LoopTools` package [27], based on [39–41] which we used for checking purposes.

The conventions we use for the scalar triangles and boxes listed below are different from the ones defined in [17,18,36,38], as we follow the LoopTools conventions for the argument lists, in order to comply with the "Les Houches Accord on Master Integrals".

To be specific, for a general N-point integral as shown in Fig. 8, we use

$$\begin{aligned} I_N^D(\{s_{j_1\ldots j_n}\};\{m_i^2\}) &= \int \frac{d^Dk}{i\,\pi^{D/2}} \frac{\mu^{4-D}}{[(k+r_1)^2-m_1^2+i\delta]\ldots[(k+r_N)^2-m_N^2+i\delta]} \qquad \text{(A.1)} \\ &= \mu^{4-D}(-1)^N\Gamma(N-\frac{D}{2})\int\limits_0^1\left(\prod_{i=1}^N dz_i\right)\frac{\delta(1-\sum_{l=1}^N z_l)}{\left(-\frac{1}{2}z_i\mathcal{S}_{ij}z_j-i\,\delta\right)^{N-\frac{D}{2}}}\,, \end{aligned}$$

where $r_i=\sum_{j=1}^i p_j$ and $\mathcal{S}_{ij}=(r_i-r_j)^2-m_i^2-m_j^2$. The results for the integrals are characterised by the invariants $s_{j_1\ldots j_n}=(p_{j_1}+\ldots+p_{j_n})^2$ and m_i^2, where the list $\{s_{j_1\ldots j_n}\}$ contains the invariants defined by n-particle cuts of the diagram. To map the labelling of $\mathcal{S}_{ij}$ resp.

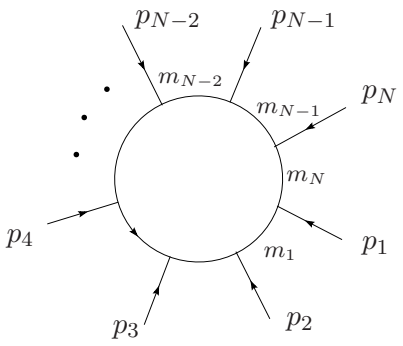

Figure 8: Momentum and mass assignments for a general N-point one-loop graph.

Fig. 8 to the LoopTools conventions, the argument lists of triangles and boxes are given by $I_3^D(s_1,s_2,s_3;m_3^2,m_1^2,m_2^2)$ and $I_4^D(s_1,s_2,s_3,s_4;s_{12},s_{23};m_4^2,m_1^2,m_2^2,m_3^2)$.

The integrals listed below will also be posted shortly to the *LoopForge* integral database at *http://www.ippp.dur.ac.uk/LoopForge*, together with some numerical benchmark points. The

triangles (A.5), (A.6), (A.8), (A.9) and the boxes (A.14), (A.15), (A.16), (A.18), (A.19) can also be found at *http://qcdloop.fnal.gov/* for certain kinematic regions.

For the analytical representations given below we use the following auxiliary functions. The Källén function:

$$\lambda(x,y,z) = x^2 + y^2 + z^2 - 2xy - 2yz - 2zx, \tag{A.2}$$

the η-function:

$$\eta(x,y) \;=\; \log(xy) - \log(x) - \log(y), \tag{A.3}$$

and the R-function [39, 40]:

$$\begin{aligned} R(y_0, z \pm i\delta) &= \int_0^1 \mathrm{d}y \frac{\log(y - z \mp i\delta) - \log(y_0 - z \mp i\delta)}{y - y_0} \\ &= \mathrm{Li}_2(z_1) - \mathrm{Li}_2(z_2) + \eta_1 \, \log(z_1) - \eta_2 \, \log(z_2) \qquad (A.4) \\ \text{where} \qquad z_1 &= \frac{y_0}{y_0 - z \mp i\delta}\,, \quad z_2 = \frac{y_0 - 1}{y_0 - z \mp i\delta} \\ \eta_1 &= \eta(-z \mp i\delta, 1/(y_0 - z \mp i\delta))\,, \quad \eta_2 = \eta(1 - z \mp i\delta, 1/(y_0 - z \mp i\delta)). \end{aligned}$$

We work in general in $D = 4 - 2\epsilon$ dimensions but give all formulas only up to $\mathcal{O}(\varepsilon^0)$. We abbreviate infinitesimal displacements in the Mandelstam variables as $\tilde{s} = s + i\delta$.

Triangle integrals

In the figures below, a single (double) internal line represents a massless (massive) propagator, while a single (double) external leg represents one for which p^2 is zero (non-zero).

Triangle $I_3^D(s_1, 0, 0; 0, 0, 0)$

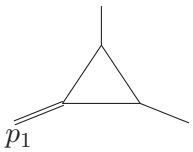

$$I_3^D(s_1, 0, 0; 0, 0, 0) = \frac{\Gamma(1+\varepsilon)}{s_1} \left[\frac{1}{\varepsilon^2} - \frac{1}{\varepsilon} \log\left(\frac{-\tilde{s}_1}{\mu^2}\right) + \frac{1}{2} \log^2\left(\frac{-\tilde{s}_1}{\mu^2}\right) - \frac{\pi^2}{6} \right] \quad . \tag{A.5}$$

Triangle $I_3^D(s_1, s_2, 0; 0, 0, 0)$

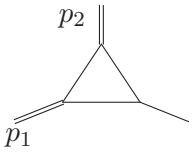

$$I_3^D(s_1, s_2, 0; 0, 0, 0) \quad = \tag{A.6}$$

$$\frac{\Gamma(1+\varepsilon)}{s_1 - s_2} \left\{ \frac{1}{\varepsilon} \left[\log\left(\frac{-\tilde{s}_2}{\mu^2}\right) - \log\left(\frac{-\tilde{s}_1}{\mu^2}\right) \right] - \frac{1}{2}\log^2\left(\frac{-\tilde{s}_2}{\mu^2}\right) + \frac{1}{2}\log^2\left(\frac{-\tilde{s}_1}{\mu^2}\right) \right\}.$$

Triangle $I_3^D(s_1, s_2, s_3; 0, 0, 0)$

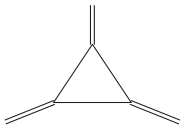

$$\begin{aligned} I_3^D(s_1, s_2, s_3; 0, 0, 0) \quad = \quad & -\frac{1}{\sqrt{\lambda(s_1, s_2, s_3) - i\delta\ s_1}} \left[2\mathrm{Li}_2\left(-\frac{x_-}{y_+}\right) + 2\mathrm{Li}_2\left(-\frac{y_-}{x_+}\right) + \frac{\pi^2}{3} \right. \\ & \left. + \frac{1}{2}\log^2\left(\frac{x_-}{y_+}\right) + \frac{1}{2}\log^2\left(\frac{y_-}{x_+}\right) + \frac{1}{2}\log^2\left(\frac{x_+}{y_+}\right) - \frac{1}{2}\log^2\left(\frac{x_-}{y_-}\right) \right] \end{aligned} \tag{A.7}$$

with

$$x_\pm \quad = \quad \frac{s_1 + s_3 - s_2 \mp \sqrt{\lambda(s_1, s_2, s_3) - i\delta\ s_1}}{2\ s_1} \quad , \quad y_\pm = 1 - x_\mp.$$

Note that the permutation symmetry of the integral in s_1, s_2, s_3 is preserved, although not manifest due to the choice of the denominator in $x_\pm$.

Triangle $I_3^D(s_1,0,0;0,M^2,0)$ 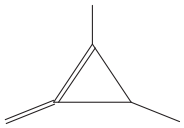

$$
\begin{aligned}
I_3^D(s_1,0,0;0,M^2,0) &= \frac{\Gamma(1+\varepsilon)}{-s_1}\left\{\frac{1}{\varepsilon}\left[\log\left(\frac{-\tilde{s}_1+M^2}{\mu^2}\right)-\log\left(\frac{M^2}{\mu^2}\right)\right]\right. \\
&\left.+\mathrm{Li}_2\left(\frac{\tilde{s}_1}{\tilde{s}_1-M^2}\right)-\frac{1}{2}\left[\log^2\left(\frac{-\tilde{s}_1+M^2}{\mu^2}\right)-\log^2\left(\frac{M^2}{\mu^2}\right)\right]\right\}
\end{aligned}
\tag{A.8}
$$

Triangle $I_3^D(s_1,s_2,0;0,M^2,0)$ 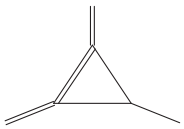

$$
\begin{aligned}
I_3^D(s_1,s_2,0;0,M^2,0) &= \frac{\Gamma(1+\varepsilon)}{s_2-s_1}\left\{\frac{1}{\varepsilon}\left[\log\left(\frac{-\tilde{s}_1+M^2}{\mu^2}\right)-\log\left(\frac{-\tilde{s}_2+M^2}{\mu^2}\right)\right]\right. \\
&+\mathrm{Li}_2\left(\frac{\tilde{s}_1}{\tilde{s}_1-M^2}\right)-\mathrm{Li}_2\left(\frac{\tilde{s}_2}{\tilde{s}_2-M^2}\right) \\
&\left.+\frac{1}{2}\log^2\left(\frac{-\tilde{s}_2+M^2}{\mu^2}\right)-\frac{1}{2}\log^2\left(\frac{-\tilde{s}_1+M^2}{\mu^2}\right)\right\}
\end{aligned}
\tag{A.9}
$$

Triangle $I_3^D(s_1,s_2,0;0,0,M^2)$ 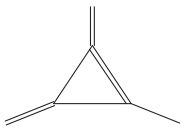

$$
\begin{aligned}
I_3^D(s_1,s_2,0;0,0,M^2) &= \frac{1}{s_2-s_1}\left\{R(x_0,\tilde{x}_1)-\frac{\pi^2}{6}+\mathrm{Li}_2\left(1-\frac{1}{x_0-i\delta}\right)\right\} \\
\text{with}\quad x_0 &= \frac{s_1}{s_1-s_2}\ ,\ \tilde{x}_1=\frac{\tilde{s}_1}{s_1-s_2+M^2}
\end{aligned}
\tag{A.10}
$$

Triangle $I_3^D(s_1, s_2, 0; 0, M^2, M^2)$ 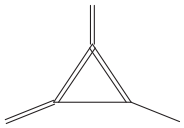

$$
\begin{aligned}
I_3^D(s_1, s_2, 0; 0, M^2, M^2) \;\; &= \\
&\frac{1}{s_2 - s_1}\left\{ \mathrm{Li}_2\left(\frac{\tilde{s}_1}{M^2}\right) - \mathrm{Li}_2\left(\frac{1}{x_+}\right) - \mathrm{Li}_2\left(\frac{1}{x_-}\right) + R\left(x_0, \frac{M^2}{\tilde{s}_1}\right) \right. \\
&\left. + R(1 - x_0, x_-) - R(x_0, x_-) - \eta_0 \log\left(\frac{1 - x_0}{-x_0}\right) \right\}
\end{aligned}
\tag{A.11}
$$

with

$$
\begin{aligned}
x_0 &= 1 - \frac{s_1}{s_2}\,,\; x_\pm = \frac{1}{2}\left(1 \pm \sqrt{1 - \frac{4M^2}{\tilde{s}_2}}\right) \\
\eta_0 &= \eta\left(1 - \frac{\tilde{s}_1}{M^2}x_0, \frac{M^2}{M^2 - \tilde{s}_2 x_0(1 - x_0)}\right)
\end{aligned}
$$

Triangle $I_3^D(s_1, s_2, s_3; 0, M^2, M^2)$ 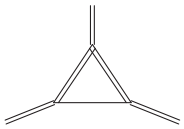

$$
\begin{aligned}
I_3^D(s_1, s_2, s_3; 0, M^2, M^2) \;\; &= \\
&\frac{1}{\sqrt{\lambda(s_1, s_2, s_3)}}\left[R(x_-, \tilde{x}_1) - R(x_+, \tilde{x}_1) + R(1 - x_-, \tilde{x}_0) - R(1 - x_+, \tilde{x}_0) \right. \\
&\left. - R(x_-, \tilde{x}_0) + R(x_+, \tilde{x}_0) - \eta_- \log\left(\frac{1 - x_-}{-x_-}\right) + \eta_+ \log\left(\frac{1 - x_+}{-x_+}\right) \right]
\end{aligned}
\tag{A.12}
$$

with

$$\begin{aligned} x_\pm &= \frac{s_1+s_2-s_3 \mp \sqrt{\lambda(s_1,s_2,s_3)}}{2s_2} \\ \tilde{x}_0 &= \frac{1}{2}\left(1-\sqrt{1-\frac{4M^2}{\tilde{s}_2}}\right)\ ,\ \tilde{x}_1 = \frac{\tilde{s}_1-M^2}{s_1-s_3} \\ \eta_\pm &= \eta\left(-s_3 x_\pm - s_1(1-x_\pm)+M^2-i\delta,\quad \frac{1}{M^2-x_\pm(1-x_\pm)\tilde{s}_2}\right)\ . \end{aligned}$$

In this formula we assume momentum conservation and at least one positive invariant s_j. The latter condition is always guaranteed if the triangle graph is a subgraph of $1 \to n$ or $2 \to n$ scattering kinematics. These lead to a positive Kaellen function: $\lambda(s_1, s_2, s_3) > 0$.

Box integrals

The results are given here for D=4-2ϵ dimensional boxes. The conversion relation to 6-dimensional boxes is achieved by the formula

$$I_4^D = \sum_{i=1}^{4} b_i\, I_{3,i}^D + (D-3)\, B\, I_4^{D+2}\ , \tag{A.13}$$

where $b_i = \sum_{j=1}^4 \mathcal{S}_{ij}^{-1}$ and $B = \sum_{i=1}^4 b_i$. $I_{3,i}^D$ denotes the "pinch" triangle stemming from a box where the ith propagator is omitted. All pinch triangle integrals needed by eq. (A.13) are given above. We use $s_{12} = s$ and $s_{23} = t$ in the following.

Box $I_4^D(s_1,0,0,0;s,t;0,0,0,0)$

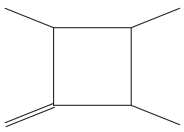

$$\begin{aligned} I_4^D(s_1,0,0,0;s,t;0,0,0,0) &= \frac{\Gamma(1+\varepsilon)}{st}\left\{\frac{2}{\varepsilon^2}-\frac{2}{\epsilon}\left[\log\left(\frac{-\tilde{s}}{\mu^2}\right)+\log\left(\frac{-\tilde{t}}{\mu^2}\right)-\log\left(\frac{-\tilde{s}_1}{\mu^2}\right)\right]\right. \\ &+2\,\mathrm{Li}_2\left(1-\frac{\tilde{s}}{\tilde{s}_1}\right)+2\,\mathrm{Li}_2\left(1-\frac{\tilde{t}}{\tilde{s}_1}\right)+2\log\left(\frac{\tilde{s}}{\tilde{s}_1}\right)\log\left(\frac{\tilde{t}}{\tilde{s}_1}\right) \\ &\left.+\log^2\left(\frac{-\tilde{s}}{\mu^2}\right)-\log^2\left(\frac{-\tilde{s}_1}{\mu^2}\right)+\log^2\left(\frac{-\tilde{t}}{\mu^2}\right)-\frac{2\pi^2}{3}\right\} \end{aligned} \tag{A.14}$$

Box $I_4^D(s_1, s_2, 0, 0; s, t; 0, 0, 0, 0)$ 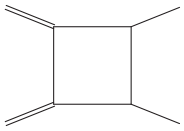

$$
\begin{aligned}
&I_4^D(s_1, s_2, 0, 0; s, t; 0, 0, 0, 0) \quad = \\
&\frac{\Gamma(1+\varepsilon)}{st}\left\{\frac{1}{\varepsilon^2}+\frac{1}{\varepsilon}\left[\log\left(\frac{-\tilde{s}_1}{\mu^2}\right)+\log\left(\frac{-\tilde{s}_2}{\mu^2}\right)-\log\left(\frac{-\tilde{s}}{\mu^2}\right)-2\log\left(\frac{-\tilde{t}}{\mu^2}\right)\right]-\frac{\pi^2}{6}\right. \\
&-2\mathrm{Li}_2\left(1-\frac{\tilde{s}_1}{\tilde{t}}\right)-2\mathrm{Li}_2\left(1-\frac{\tilde{s}_2}{\tilde{t}}\right)+\log\left(\frac{\tilde{s}}{\tilde{s}_1}\right)\log\left(\frac{\tilde{s}}{\tilde{s}_2}\right) \\
&\left.-\log^2\left(\frac{\tilde{s}}{\tilde{t}}\right)+\frac{1}{2}\log^2\left(\frac{-\tilde{s}}{\mu^2}\right)-\frac{1}{2}\log^2\left(\frac{-\tilde{s}_1}{\mu^2}\right)-\frac{1}{2}\log^2\left(\frac{-\tilde{s}_2}{\mu^2}\right)+\log^2\left(\frac{-\tilde{t}}{\mu^2}\right)\right\}
\end{aligned}
\tag{A.15}
$$

Box $I_4^D(s_1, 0, s_3, 0; s, t; 0, 0, 0, 0)$ 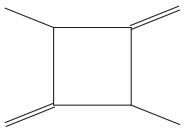

$$
\begin{aligned}
&I_4^D(s_1, 0, s_3, 0; s, t; 0, 0, 0, 0) \quad = \\
&\frac{\Gamma(1+\varepsilon)}{st-s_1s_3}\left\{\frac{2}{\epsilon}\left[\log\left(\frac{-\tilde{s}_1}{\mu^2}\right)+\log\left(\frac{-\tilde{s}_3}{\mu^2}\right)-\log\left(\frac{-\tilde{s}}{\mu^2}\right)-\log\left(\frac{-\tilde{t}}{\mu^2}\right)\right]\right. \\
&+\log^2\left(\frac{-\tilde{s}}{\mu^2}\right)-\log^2\left(\frac{-\tilde{s}_1}{\mu^2}\right)-\log^2\left(\frac{-\tilde{s}_3}{\mu^2}\right)+\log^2\left(\frac{-\tilde{t}}{\mu^2}\right) \\
&-2\,\mathrm{Li}_2\left(1-\frac{\tilde{s}_1}{\tilde{s}}\right)-2\,\mathrm{Li}_2\left(1-\frac{\tilde{s}_3}{\tilde{s}}\right)-2\,\mathrm{Li}_2\left(1-\frac{\tilde{s}_1}{\tilde{t}}\right)-2\,\mathrm{Li}_2\left(1-\frac{\tilde{s}_3}{\tilde{t}}\right) \\
&\left.+2\,\mathrm{Li}_2\left(1-\frac{\tilde{s}_1\,\tilde{s}_3}{\tilde{s}\,\tilde{t}}\right)-\log^2\left(\frac{\tilde{s}}{\tilde{t}}\right)+2\,\eta\left(\frac{\tilde{s}_3}{\tilde{s}},\frac{\tilde{s}_1}{\tilde{t}}\right)\log\left(1-\frac{\tilde{s}_1\,\tilde{s}_3}{\tilde{s}\,\tilde{t}}\right)\right\}
\end{aligned}
\tag{A.16}
$$

Box $I_4^D(s_1,0,0,0;s,t;0,M^2,0,0)$ 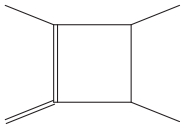

We find for the 6-dimensional integral

$$\begin{aligned} I_4^{D+2}(s_1,0,0,0;s,t;0,M^2,0,0) \;\; = \;\; & \\ & \frac{-t+M^2}{t(s_1-s-t)}\left[R\left(x_0,\tilde{x}_2\right)+\mathrm{Li}_2\left(1-\frac{1}{\tilde{x}_0}\right)-\frac{\pi^2}{6}\right] \\ & -\frac{M^2}{t(s_1-s)}\left[R\left(x_1,\tilde{x}_2\right)+\mathrm{Li}_2\left(1-\frac{1}{\tilde{x}_1}\right)-\frac{\pi^2}{6}\right] \end{aligned} \tag{A.17}$$

where

$$\begin{aligned} x_0 = \frac{s}{s+t-s_1} \quad , \quad \tilde{x}_0 = x_0 + \frac{i\delta}{t-M^2} \; , \\ x_1 = \frac{s}{s-s_1} \quad , \quad \tilde{x}_1 = x_1 - i\delta \;\; , \;\; \tilde{x}_2 = \frac{\tilde{s}}{s-s_1+M^2} \end{aligned}$$

The integral in $D = 4-2\epsilon$ is obtained by

$$\begin{aligned} I_4^D(s_1,0,0,0;s,t;0,M^2,0,0) \;\; = \;\; & b_1\, I_3(s,0,0;0,0,0) + b_2\, I_3(s_1,t,0;0,M^2,0) \\ & + b_3\, I_3(s_1,0,s;0,M^2,0) + b_4\, I_3(t,0,0;0,M^2,0) + B\, I_4^{D+2}(s_1,0,0,0;s,t;0,M^2,0,0) \end{aligned} \tag{A.18}$$

with

$$\begin{aligned} b_1 \;\; &= \;\; -\frac{1}{M^2-t} \; , \; b_2 = \frac{s_1-t}{s\,(M^2-t)} \; , \; b_3 = \frac{t(s-s_1)+M^2(s+2t-s_1)}{s\,(M^2-t)^2} \\ b_4 \;\; &= \;\; -\frac{t}{s\,(M^2-t)} \; , \; B = \frac{2\,t\,(s+t-s_1)}{s\,(M^2-t)^2} \; . \end{aligned}$$

Box $I_4^D(s_1,s_2,0,0;s,t;0,M^2,M^2,0)$ 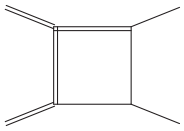

$$I_4^D(s_1,s_2,0,0;s,t;0,M^2,M^2,0) \;=\; \frac{I_{\rm pole}+I_{\rm finite}}{st-(s+t-s_1)M^2} \tag{A.19}$$

with

$$\begin{aligned}
I_{\rm pole} &= -\frac{\Gamma(1+\epsilon)}{\epsilon}\Big[\log\left(\frac{-\tilde t+M^2}{M^2}\right)-\log\left(\frac{-\tilde s_1+M^2}{-\tilde s+M^2}\right)\Big]\\
I_{\rm finite} &= \log^2\left(\frac{-\tilde t+M^2}{\mu^2}\right)-\log^2\left(\frac{M^2}{\mu^2}\right)-\log^2\left(\frac{-\tilde s_1+M^2}{\mu^2}\right)+\log^2\left(\frac{-\tilde s+M^2}{\mu^2}\right)\\
&\quad -2\,R(x_0,\tilde x_1)+2\,R(x_0,\tilde x_2)\\
&\quad +R(1-x_1,x_-)-R(x_1,x_-)-R(1-x_2,x_-)+R(x_2,x_-)\\
&\quad -\Big[\log\left(-\tilde s_2/\mu^2\right)+\log(x_+-x_1)+\log(x_1-x_-)\Big]\log\left(\frac{1-\tilde x_1}{-\tilde x_1}\right)\\
&\quad +\Big[\log\left(-\tilde s_2/\mu^2\right)+\log(x_+-x_2)+\log(x_2-x_-)\Big]\log\left(\frac{1-\tilde x_2}{-\tilde x_2}\right)\\
x_\pm &= \frac{1}{2}\left(1\pm\sqrt{1-\frac{4M^2}{\tilde s_2}}\right)\quad,\quad x_0=\frac{s}{s+t-s_1}\\
x_1 &= \frac{M^2}{t}\quad,\quad \tilde x_1=\frac{M^2-i\delta}{t}\quad,\quad x_2=\frac{s-M^2}{s-s_1}\quad,\quad \tilde x_2=\frac{\tilde s-M^2}{s-s_1}
\end{aligned}$$

Box $I_4^D(s_1,0,s_3,0;s,t;0,0,M^2,M^2)$: 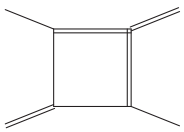

$$I_4^D(s_1,0,s_3,0;s,t;0,0,M^2,M^2) \;=\; \frac{I_- - I_+}{\sqrt{\det(\mathcal{S})-Ji\delta}} \tag{A.20}$$

with the auxiliary integrals[3]

$$
\begin{aligned}
I_\pm &= R\left(x_\pm, \frac{M^2}{\tilde{t}}\right) - R\left(1-x_\pm, \frac{M^2}{\tilde{s}}\right) + R(1-x_\pm, x_0^-) - R(x_\pm, x_0^-) \\
&\quad + \log\left(\frac{1-x_\pm}{-x_\pm}\right)\left[\log\left(\frac{\tilde{s}}{\tilde{s}_1}\right) + \log\left(\frac{\tilde{t}}{\tilde{s}_3}\right) + \log\left(x_\pm - \frac{M^2}{\tilde{t}}\right)\right. \\
&\quad \left. - \log(x_0^+ - x_\pm) - \log(x_\pm - x_0^-) + \log\left(1 - x_\pm - \frac{M^2}{\tilde{s}}\right)\right] \qquad \text{(A.21)}
\end{aligned}
$$

where

$$
\begin{aligned}
\det(\mathcal{S}) &= [st - s_1 s_3 + M^2(s-t)]^2 + 4M^2(st - s_1 s_3)(-s + s_1 + M^2) \\
J &= 2(s_3 - t)[st - s_1 s_3 + M^2(s-t)] + 4(st - s_1 s_3)(-s + s_1 + M^2), \\
x_\pm &= \frac{(st - s_1 s_3) + M^2(s-t) \pm \sqrt{\det(\mathcal{S}) - Ji\delta}}{2\,(st - s_1 s_3)} \;\;,\;\; x_0^\pm = \frac{1}{2}\left(1 \pm \sqrt{1 - \frac{4M^2}{\tilde{s}_3}}\right)
\end{aligned}
$$

Checks on the integrals

We tested the Master Integrals by comparing our results numerically with `LoopTools` [27]. For the IR finite box and triangle integrals this is straightforward. The IR divergent box integrals have been checked indirectly by mapping to the 6D case which is IR finite. Using eq. (A.13) the $1/\varepsilon$ poles cancel when combining the D-dimensional box with the triangle pinch integrals. The same expression can be evaluated with `LoopTools` by using a mass regulators in the IR divergent integrals. In the given IR finite combinations the cut-off dependence is polynomial and can be made arbitrarily small. We have tested the formulae in all kinematically distinguishable regions. For example, $I_3^D(s_1, s_2, s_3; 0, M^2, M^2)$ has been checked in the regions resulting from combining the conditions ($s_1 < 0$, $0 < s_1 < M^2$, $M^2 < s_1$), ($s_2 < 0$, $0 < s_2 < 4\,M^2$, $4\,M^2 < s_2$) and ($s_3 < 0$, $0 < s_3 < M^2$, $M^2 < s_3$) such that the Kaellen function is positive in line with the comment below equation (A.12).

References

[1] S. Y. Choi, D. J. Miller, M. M. Muhlleitner, and P. M. Zerwas, *Identifying the Higgs spin and parity in decays to Z pairs*, *Phys. Lett.* **B553** (2003) 61–71, [hep-ph/0210077].

[2] D. L. Rainwater and D. Zeppenfeld, *Observing $H \to W^{(*)}W^{(*)} \to e^\pm\mu^\mp \not{p}_T$ in weak boson fusion with dual forward jet tagging at the CERN LHC*, *Phys. Rev.* **D60** (1999) 113004, [hep-ph/9906218].

[3] The $\pm$ label of the integrals $I_\pm$ are related to $x_\pm$. The exchange of $\pm$ has no effect on x_0^- and x_0^+.

[3] R. N. Cahn and S. Dawson, *Production of very massive Higgs bosons*, *Phys. Lett.* **B136** (1984) 196.

[4] D. A. Dicus and S. S. D. Willenbrock, *Higgs bosons from vector boson fusion in e+ e-, e p and p p collisions*, *Phys. Rev.* **D32** (1985) 1642.

[5] G. Altarelli, B. Mele, and F. Pitolli, *Heavy higgs production at future colliders*, *Nucl. Phys.* **B287** (1987) 205–224.

[6] T. Plehn, D. L. Rainwater, and D. Zeppenfeld, *Determining the structure of Higgs couplings at the LHC*, *Phys. Rev. Lett.* **88** (2002) 051801, [hep-ph/0105325].

[7] J. M. Campbell, R. Keith Ellis, and G. Zanderighi, *Next-to-leading order Higgs + 2 jet production via gluon fusion*, *JHEP* **10** (2006) 028, [hep-ph/0608194].

[8] V. Del Duca, A. Frizzo, and F. Maltoni, *Higgs boson production in association with three jets*, *JHEP* **05** (2004) 064, [hep-ph/0404013].

[9] F. Wilczek, *Decays of Heavy Vector Mesons Into Higgs Particles*, *Phys. Rev. Lett.* **39** (1977) 1304.

[10] S. Dawson, *Radiative corrections to higgs boson production*, *Nucl. Phys.* **B359** (1991) 283–300.

[11] A. Djouadi, M. Spira, and P. M. Zerwas, *Production of higgs bosons in proton colliders: Qcd corrections*, *Phys. Lett.* **B264** (1991) 440–446.

[12] T. Han, G. Valencia, and S. Willenbrock, *Structure function approach to vector boson scattering in p p collisions*, *Phys. Rev. Lett.* **69** (1992) 3274–3277, [hep-ph/9206246].

[13] T. Figy, C. Oleari, and D. Zeppenfeld, *Next-to-leading order jet distributions for Higgs boson production via weak-boson fusion*, *Phys. Rev.* **D68** (2003) 073005, [hep-ph/0306109].

[14] E. L. Berger and J. Campbell, *Higgs boson production in weak boson fusion at next-to-leading order*, *Phys. Rev.* **D70** (2004) 073011, [hep-ph/0403194].

[15] M. Ciccolini, A. Denner, and S. Dittmaier, *Strong and electroweak corrections to the production of Higgs+2jets via weak interactions at the LHC*, 0707.0381.

[16] J. R. Andersen and J. M. Smillie, *QCD and electroweak interference in Higgs production by gauge boson fusion*, *Phys. Rev.* **D75** (2007) 037301, [hep-ph/0611281].

[17] T. Binoth, J. P. Guillet, and G. Heinrich, *Reduction formalism for dimensionally regulated one-loop N- point integrals*, *Nucl. Phys.* **B572** (2000) 361–386, [hep-ph/9911342].

[18] T. Binoth, J. P. Guillet, G. Heinrich, E. Pilon, and C. Schubert, *An algebraic / numerical formalism for one-loop multi-leg amplitudes*, *JHEP* **10** (2005) 015, [hep-ph/0504267].

[19] T. Binoth, M. Ciccolini, N. Kauer, and M. Kramer, *Gluon-induced w-boson pair production at the lhc*, *JHEP* **12** (2006) 046, [hep-ph/0611170].

[20] T. Binoth, S. Karg, N. Kauer, and R. Ruckl, *Multi-higgs boson production in the standard model and beyond*, *Phys. Rev.* **D74** (2006) 113008, [hep-ph/0608057].

[21] T. Binoth, M. Ciccolini, N. Kauer, and M. Kramer, *Gluon-induced W W background to Higgs boson searches at the LHC*, *JHEP* **03** (2005) 065, [hep-ph/0503094].

[22] T. Binoth, J. P. Guillet, and F. Mahmoudi, *A compact representation of the gamma gamma g g g $\longrightarrow$ 0 amplitude*, *JHEP* **02** (2004) 057, [hep-ph/0312334].

[23] J. A. M. Vermaseren, *New features of FORM*, math-ph/0010025.

[24] Wolfram Research, Inc., *Mathematica*. 5.2 ed., 2005.

[25] L. J. Dixon and Y. Sofianatos. in preparation.

[26] T. Binoth, G. Heinrich, T. Gehrmann, and P. Mastrolia, *Six-photon amplitudes*, *Phys. Lett.* **B649** (2007) 422–426, [hep-ph/0703311].

[27] T. Hahn and M. Perez-Victoria, *Automatized one-loop calculations in four and d dimensions*, *Comput. Phys. Commun.* **118** (1999) 153–165, [hep-ph/9807565].

[28] W. T. Giele and E. W. N. Glover, *Higher order corrections to jet cross-sections in e+ e- annihilation*, *Phys. Rev.* **D46** (1992) 1980–2010.

[29] W. T. Giele, E. W. N. Glover, and D. A. Kosower, *Higher order corrections to jet cross-sections in hadron colliders*, *Nucl. Phys.* **B403** (1993) 633–670, [hep-ph/9302225].

[30] V. Del Duca, W. Kilgore, C. Oleari, C. Schmidt, and D. Zeppenfeld, *Gluon-fusion contributions to H + 2 jet production*, *Nucl. Phys.* **B616** (2001) 367–399, [hep-ph/0108030].

[31] A. D. Martin, R. G. Roberts, W. J. Stirling, and R. S. Thorne, *Physical gluons and high-E(T) jets*, *Phys. Lett.* **B604** (2004) 61–68, [hep-ph/0410230].

[32] W.-M. Yao *et. al.*, *Review of Particle Physics*, *Journal of Physics G* **33** (2006).

[33] V. Hankele, G. Klamke, D. Zeppenfeld, and T. Figy, *Anomalous Higgs boson couplings in vector boson fusion at the CERN LHC*, *Phys. Rev.* **D74** (2006) 095001, [hep-ph/0609075].

[34] J. R. Forshaw and M. Sjodahl, *Soft gluons in Higgs plus two jet production*, 0705.1504.

[35] V. Del Duca *et. al.*, *Monte carlo studies of the jet activity in higgs + 2jet events*, *JHEP* **10** (2006) 016, [hep-ph/0608158].

[36] Z. Bern, L. J. Dixon, and D. A. Kosower, *Dimensionally regulated one loop integrals*, *Phys. Lett.* **B302** (1993) 299–308, [hep-ph/9212308].

[37] H. J. Lu and C. A. Perez, *Massless one loop scalar three point integral and associated Clausen, Glaisher and L functions*, . SLAC-PUB-5809.

[38] Z. Bern, L. J. Dixon, and D. A. Kosower, *Dimensionally regulated pentagon integrals*, *Nucl. Phys.* **B412** (1994) 751–816, [hep-ph/9306240].

[39] G. 't Hooft and M. J. G. Veltman, *Scalar one loop integrals*, *Nucl. Phys.* **B153** (1979) 365–401.

[40] G. J. van Oldenborgh and J. A. M. Vermaseren, *New algorithms for one loop integrals*, *Z. Phys.* **C46** (1990) 425–438.

[41] A. Denner, U. Nierste, and R. Scharf, *A compact expression for the scalar one loop four point function*, *Nucl. Phys.* **B367** (1991) 637–656.